Analysis of the Fluorescence Spectrum of $LiYF_4:Eu^{3+}$

C. GÖRLLER-WALRAND, M. BEHETS

University of Leuven, Laboratory of Inorganic Chemistry, Celestijnenlaan 200F, 3030 Heverlee, Belgium

P. PORCHER, O. K. MOUNE-MINN

Laboratoire des éléments de transition dans les solides, E.R. 210 du CNRS, 1 Place A. Briand, F 92195 Meudon Principal Cedex, France

and I. LAURSEN

Department of Electrophysics, The Technical University of Denmark, DK 2800 Lyngby, Denmark

Received August 24, 1984

Abstract

The fluorescence spectrum of the scheelite-type $LiYF_4/Eu^{3+}$ crystal was analyzed and accurately described by a set of crystal field parameters in a S_4 – not far from D_{2d} – symmetry.

Introduction

Compounds with Scheelite-like structure have in the past been the subject of many spectroscopic investigations, as well as *ab initio* calculations [1]. $LiYF_4$ has been studied as a promising efficient laser when doped by various rare earths, mainly by Nd^{3+}. A complete survey of the actual results is found in reference [2].

The symmetry of the point site, S_4 – not far from D_{2d} –, constitutes a sensitive case where various magneto-optical features can be precisely studied, due to the relatively small number of phenomenological parameters involved. This work was performed in order to characterize the optical properties of a single crystal of $LiYF_4:Eu^{3+}$.

From the fluorescence spectrum the crystal field parameters (c.f.p.) were calculated and the wavefunctions were derived in view of a future precise simulation of the magnetic circular dichroism (MCD) [3, 4] spectra.

Experimental

Preparation and Structure of the $LiYF_4/Eu^{3+}$ Compound

Method of synthesis

Crystals of $LiYF_4$, doped with Eu^{3+}, were grown by spontaneous nucleation in the melt [5].

As starting materials, high purity LiF and EuF_3 (99.99%), and anhydrous YF_3 (99.9999%) were used. According to the mole weight relations between YF_3 and EuF_3, the doping concentration of the $LiYF_4:Eu^{3+}$ crystals is 5.00 ± 0.05%.

By indirect cooling of the crucible bottom, the temperature gradient in the melt was increased during the growth, thereby improving size and quality of crystals.

Possible contaminations of the melt are LiF, YF_3, EuF_3, YOF and EuOF. However, analysis of the melt by Debye-Sherrer exposures and polarized light microscope did not reveal any foreign phases. Furthermore, the transparency of the sample indicates a high purity, because even small amounts of wrong phases (10 ppm) would lead to severe decrease of optical transmission.

For the rare earths (Ln^{3+}), the yttrium-ion will be substituted, partially or wholly, by a lanthanide ion.

Due to a destructive Ln^{3+}–Ln^{3+} interaction, the doping percentage may not exceed 5% for the case of Eu^{3+}, if growth of large, perfect crystals is wanted.

Structure [11]

The $LiYF_4$ crystals are uniaxial hosts, belonging to the tetragonal scheelite structure (space group C_{4h}^6).

The polyhedron, formed by the nearest surrounders of the rare earth ions, eight fluorides (F^-), is nearly a dodecahedron.

The crystallographic point site symmetry is D_{2d}, slightly distorted to a S_4-symmetry; this implies a distortion of the ϕ coordinates from the dodecahedron D_{2d} values [6].

Spectroscopic Measurements

The fluorescence of the $LiYF_4$:5% Eu^{3+} was excited by an ORIEL 200 W mercury lamp, equipped

0020-1693/85/$3.30

TABLE I. Selection Rules for Electric and Magnetic Dipole Transitions (in Kosters and Cottons Notation).

$D_{2d_{E.D.}}$	$\Gamma_1(A_1)$	$\Gamma_2(A_2)$	$\Gamma_3(B_1)$	$\Gamma_4(B_2)$	$\Gamma_5(E)$
Γ_1	–	–	–	π	σ
Γ_2	–	–	π	–	σ
Γ_3	–	π	–	–	σ
Γ_4	π	–	–	–	σ
Γ_5	σ	σ	σ	σ	π

$D_{2d_{M.D.}}$	Γ_1	Γ_2	Γ_3	Γ_4	Γ_5
Γ_1	–	σ	–	–	π
Γ_2	σ	–	–	–	π
Γ_3	–	–	–	σ	π
Γ_4	–	–	σ	–	π
Γ_5	π	π	π	π	σ

$S_{4_{E.D.}}$	$\Gamma_1(A)$	$\Gamma_2(B)$	$\Gamma_{3,4}(E)$
Γ_1	–	π	σ
Γ_2	π	–	σ
$\Gamma_{3,4}$	σ	σ	π

$S_{4_{M.D.}}$	Γ_1	Γ_2	$\Gamma_{3,4}$
Γ_1	σ	–	π
Γ_2	–	σ	π
$\Gamma_{3,4}$	π	π	σ

with wide band long-UV filters. The UV-light was focussed on the sample, immersed in liquid nitrogen (77 K), and the reflected light entered a 1 m Jarrel-Ash monochromator having a resolution of about 0.1 Å.

Alternatively, to obtain the selective excitation of the $^5D_0$-level of Eu^{3+}, a Rhodamin 6 G dye laser coupled to a 4 W Ar-ion laser was used. Because of the fact that the $^5D_0 \rightarrow {}^7F_0$ transition is forbidden in the considered symmetry, the selective excitation cannot be performed through this transition. However, when the laser is tuned to the $^5D_0 \rightarrow {}^7F_1$ transitions at 77 K, the remaining thermal population of the lowest $^7F_1$ Stark level (±0.5%) is sufficient to excite $^5D_0 \leftarrow {}^7F_1$. The analysed wavelength region varied between 14200 cm^{-1} and 20800 cm^{-1} corresponding to the transitions ^5D_J (J = 0,1,2) $\rightarrow {}^7F_J$ (J = 0,1,2,3,4,5) of Eu^{3+}.

Because of the fact that the fluorescence measurements were unpolarised, the orientation of the crystal with respect to the incident light was unimportant. In the present case, the optical axis was lying in the plane of the crystal.

Selection Rules for Transitions

In a crystal the $^{2S+1}L_J$ levels of the Eu^{3+} are split into several Stark sublevels according to their J-value [7].

As from the previous section it appears that a small distortion from D_{2d} to S_4 has to be taken into account, the two symmetries are considered and labels are given accordingly to the Koster [7] and Cotton [8] notations.

In Table I the selection rules for electric and magnetic dipole transitions are summarized.

Analysis of the Fluorescence Spectra

(i) The transitions having different emitting levels towards the same final level appear on the spectrum as a group of peaks which will appear as a same group of homologous peaks when transition to another final level is considered.

(ii) Although the selection rules give spectra compatible with a S_4 pointgroup, the relative weakness of certain levels suggests that the site symmetry is not far from D_{2d}. This remark is of interest for the simulation of the energy level positions because some irreducible representations differ for the two groups, as well as electronic transition selection rules. For instance the $\Gamma_1(A)$ and $\Gamma_2(B)$ are undifferentiated in S_4 but split respectively into $\Gamma_1(A_1) - \Gamma_2(A_2)$ and $\Gamma_3(B_1) - \Gamma_4(B_2)$ in D_{2d}. This will help for the attribution of the irreducible representation and fix the relative sign of B_4^4 and B_4^6.

Region 19050–19000 cm^{-1} (Fig. 1a) $^5D_1 \rightarrow {}^7F_0$

The two peaks correspond to magnetic dipole transitions from Γ_1 and $\Gamma_{3,4}$ (S_4) of $^5D_1$ to the Γ_1 (S_4) ground state ($^7F_0$) in respectively σ- and π-polarisation. The energy separation between Γ_1 and $\Gamma_{3,4}$ is 21 cm^{-1}.

Region 18800–18500 cm^{-1} and 16950–16800 cm^{-1} (Fig. 1a, 1b) $\rightarrow {}^7F_1$

The peaks at 16840 cm^{-1} and 16395 cm^{-1} correspond to the magnetic dipole $^5D_0 \rightarrow {}^7F_1$ transition, respectively $\Gamma_1 \rightarrow \Gamma_1$ (S_4) and $\Gamma_1 \rightarrow \Gamma_{3,4}$. The energy separation of 95 cm^{-1} helps to assign the three intense peaks in the region 18800–18000 cm^{-1}. They correspond to the $^5D_1 \rightarrow {}^7F_1$ transition, which is both magnetic and electric dipole allowed. The weak shoulder at 18601 cm^{-1} is probably the $\Gamma_1 \rightarrow \Gamma_1$ magnetic dipole σ-transition.

Region 18200–17800 cm^{-1} and 16500–15900 cm^{-1} (Fig. 1a, 1b and 2) $\rightarrow {}^7F_2$

This region corresponds respectively to the $^5D_1 \rightarrow {}^7F_2$ transition and to a superposition of the $^5D_0 \rightarrow {}^7F_2$ and $^5D_1 \rightarrow {}^7F_4$ transitions.

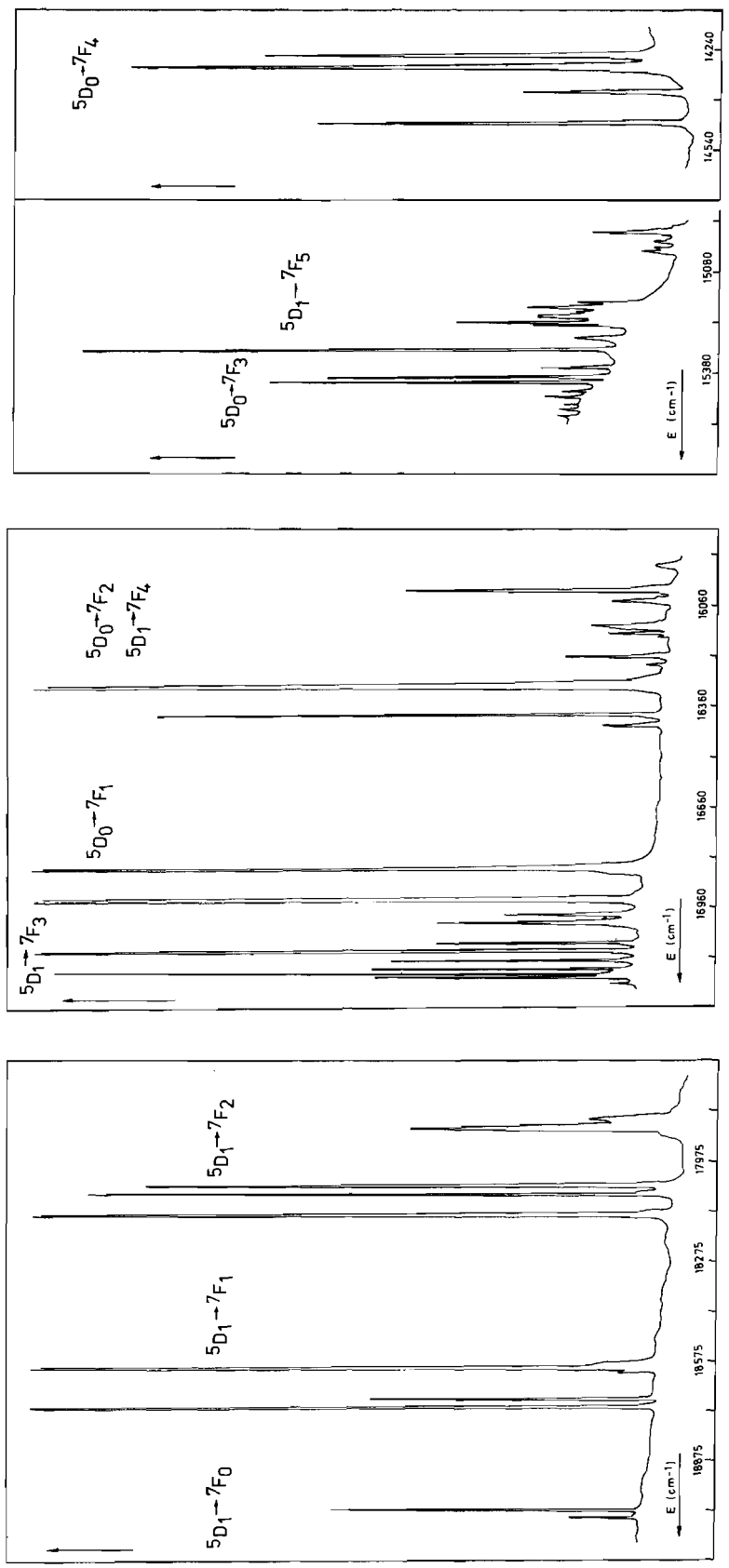

Fig. 1a,b,c. Fluorescence spectra of the $LiYF_4/Eu^{3+}$ recorded by excitation with a 200 W Mercury lamp. (The scale in ordinate is arbitrary and varies for each wavelength region).

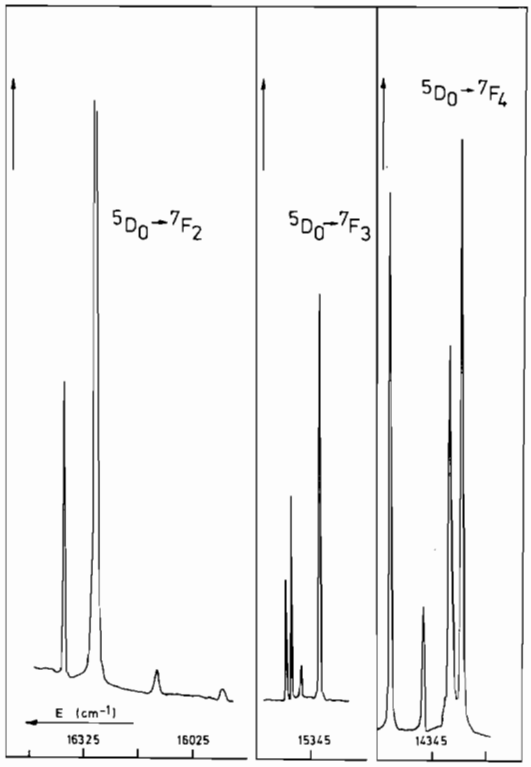

Fig. 2. Fluorescence spectra of the $LiYF_4/Eu^{3+}$ for selective excitation of the $^5D_0$-level by a Rhodamin 6 G dye laser coupled to a 4 W Ar-ion laser. (The scale in ordinate is arbitrary and varies for each wavelength region).

With the laser excitation only the $^5D_0 \rightarrow {}^7F_2$ is seen, allowing us to identify the components at 16120 cm^{-1}, 16293 cm^{-1} and 16379 cm^{-1} as belonging to this transition. The weak peak at 16120 cm^{-1} can be unambiguously associated to the $\Gamma_1 \rightarrow \Gamma_2$ Stark component, because this transition is due to the slight distortion from D_{2d} to S_4 ($\Gamma_1 \rightarrow \Gamma_3$ is electric-dipole forbidden in D_{2d}). The weak signal at 15938 cm^{-1} probably has its origin in a vibronic transition mechanism (associated with $^5D_0 \rightarrow {}^7F_2$: $\bar{\nu} \simeq 350$ cm^{-1}).

The $^5D_1 \rightarrow {}^7F_2$ (Fig. 2a) helps to assign the two remaining peaks in providing the possibility to position the Γ_1 level belonging to $^7F_2$ at 1172 cm^{-1} above the groundstate. Indeed, in the region 17800 cm^{-1}–18200 cm^{-1} the twins can be associated with the magnetic dipole transition from the Γ_1 and $\Gamma_{3,4}$ levels of $^5D_1$ to the Γ_2 and $\Gamma_{3,4}$ levels of $^7F_2$. The fifth peak at 18129 cm^{-1} corresponds to the $\Gamma_{3,4}$ to Γ_2 while the expected second $\Gamma_{3,4} \rightarrow \Gamma_2$ transition is superposed on the $\Gamma_1 \rightarrow \Gamma_1$ transition.

The 17891 cm^{-1} peak could be the weakly allowed electric dipole transition $\Gamma_1 \rightarrow \Gamma_2$.

Region 17200–16950 cm^{-1} and 15420–15320 cm^{-1} (Fig. 1b, 1c and 2) $\rightarrow {}^7F_3$

This region corresponds to the $^5D_1 \rightarrow {}^7F_3$ and $^5D_0 \rightarrow {}^7F_3$ fluorescence. The Stark splitting of the $^7F_3$ level occurs following Γ_1, $2\Gamma_2$ and $2\Gamma_{3,4}$ in S_4 and Γ_1, Γ_3 and $2\Gamma_5$ in D_{2d}.

From the $^5D_0$ (Γ_1), transitions will be both electric and magnetic dipole allowed.

If in first approximation only the D_{2d}-symmetry is considered, four kinds of possibilities occur, namely from Γ_1 to Γ_2, Γ_4 and Γ_5 (2X). This is found experimentally, leading to the positions at 15317 cm^{-1} (Γ_2), 15367 cm^{-1} (Γ_4), 15397 cm^{-1} (Γ_5) and 15411 cm^{-1} (Γ_5).

Remaining transitions, due to the slight distortion to S_4, are hardly seen and will be weakly allowed.

Concerning the $^5D_1 \rightarrow {}^7F_3$, the expectations for an electric dipole transition are: from Γ_2 to Γ_3 and Γ_5 (2 X), and from Γ_5 to all Γ_i (Γ_2, Γ_3, Γ_4 and $2 \times \Gamma_5$).

Experimentally there are two groups of three peaks, separated by 21 cm^{-1}, which would correspond to the electric dipole transitions Γ_2 to Γ_3 and Γ_5 (2 X) in D_{2d}. Besides, the two lone peaks can be associated with the transition from Γ_5 to Γ_4 and Γ_2.

If it is assumed that the transitions have mainly an electric dipole character, the distortion to S_4 would allow to some extent the $\Gamma_1 \rightarrow \Gamma_2$ which is forbidden in D_{2d} ($\Gamma_2 \rightarrow \Gamma_4$).

Region 14200–14500 cm^{-1} and 15900–16500 cm^{-1} (Fig. 1b, 1c and 2) $\rightarrow {}^7F_4$

The region 15900 cm^{-1}–16500 cm^{-1} corresponds to a superposition of $^5D_1 \rightarrow {}^7F_4$ and $^5D_0 \rightarrow {}^7F_2$; with laser excitation, one obtains the identification of the four peaks of the $^5D_0 \rightarrow {}^7F_2$ transition. The remaining nine signals give the emission from the $^5D_1$ level.

The Stark splitting of the $^7F_4$ multiplet results in $2 \times \Gamma_1$, Γ_2, Γ_3, Γ_4 and $2 \times \Gamma_5$ in D_{2d}, and $3 \times \Gamma_1$, $2 \times \Gamma_2$ and $2 \times \Gamma_{3,4}$ in S_4.

Following the electric dipole transition rules one should obtain three peaks in D_{2d} and four in S_4 for the $^5D_0 \rightarrow {}^7F_4$ transition. Experimentally, three intense signals and one weak signal are seen. This last one is in agreement with the allowed $\Gamma_1 \rightarrow \Gamma_2$ transition in S_4 (forbidden $\Gamma_1 \rightarrow \Gamma_3$ in D_{2d}).

The differentiation between the Γ_2 and $\Gamma_{3,4}$ representations (in S_4) and the position of the three remaining Γ_1 representations can be made by the interpretation of the $^5D_1 \rightarrow {}^7F_4$ transition. The spectrum gives three pairs of peaks associated with the Γ_1 and $\Gamma_{3,4}$ to Γ_2 and $\Gamma_{3,4}$ transitions. Two of the three observed lone peaks are characterized as $\Gamma_{3,4} \rightarrow \Gamma_1$ transitions (16149 cm^{-1} and 16413 cm^{-1}).

The signal at 16402 cm^{-1} can be explained by a $\Gamma_{3,4}$ to Γ_2 transition. In theory one should expect

TABLE II. Identification of the Electronic Transitions of $LiYF_4/Eu^{3+}$.

Transition	$\bar{\nu}$ (cm^{-1})	Polarisation and mechanism	Identification	
			S_4	D_{2d}
$^5D_0 \rightarrow {}^7F_4$	14257	ED σ	$\Gamma_1 \rightarrow \Gamma_{3,4}$	$\Gamma_1 \rightarrow \Gamma_5$
	14291	ED π	$\Gamma_1 \rightarrow \Gamma_2$	$\Gamma_1 \rightarrow \Gamma_4$
	14365	ED π	$\Gamma_1 \rightarrow \Gamma_2$	$\Gamma_1 \rightarrow \Gamma_3$
	14458	ED σ	$\Gamma_1 \rightarrow \Gamma_{3,4}$	$\Gamma_1 \rightarrow \Gamma_5$
$^5D_1 \rightarrow {}^7F_5$	14949	ED σ	$\Gamma_{3,4} \rightarrow \Gamma_2$	$\Gamma_5 \rightarrow \Gamma_4$
	14969	ED π, ED π	$(\Gamma_1 \rightarrow \Gamma_2)/\Gamma_{3,4} \rightarrow \Gamma_{3,4}$	$(\Gamma_2 \rightarrow \Gamma_4)/\Gamma_5 \rightarrow \Gamma_5$
	14982	ED σ	$\Gamma_{3,4} \rightarrow \Gamma_1$	$\Gamma_5 \rightarrow \Gamma_1/\Gamma_2$
	14991	ED σ	$\Gamma_1 \rightarrow \Gamma_{3,4}$	$\Gamma_2 \rightarrow \Gamma_5$
	15014	ED σ	$\Gamma_{3,4} \rightarrow \Gamma_1$	$\Gamma_5 \rightarrow \Gamma_1/\Gamma_2$
	15021	ED π	$\Gamma_{3,4} \rightarrow \Gamma_{3,4}$	$\Gamma_5 \rightarrow \Gamma_5$
	15176	ED σ	$\Gamma_{3,4} \rightarrow \Gamma_1$	$\Gamma_5 \rightarrow \Gamma_2$
	15188	ED σ		
	15201			
	15212	ED π	$\Gamma_{3,4} \rightarrow \Gamma_{3,4}$	$\Gamma_5 \rightarrow \Gamma_5$
	15224	ED σ	$\Gamma_{3,4} \rightarrow \Gamma_2$	$\Gamma_5 \rightarrow \Gamma_3$
	15234	ED σ	$\Gamma_1 \rightarrow \Gamma_{3,4}$	$\Gamma_2 \rightarrow \Gamma_5$
	15245	ED π	$\Gamma_1 \rightarrow \Gamma_2$	$\Gamma_2 \rightarrow \Gamma_3$
	15282			
$^5D_0 \rightarrow {}^7F_3$	15317	ED σ, MD π	$\Gamma_1 \rightarrow \Gamma_{3,4}$	$\Gamma_1 \rightarrow \Gamma_5$
	15367	MD σ	$\Gamma_1 \rightarrow \Gamma_1$	$\Gamma_1 \rightarrow \Gamma_2$
	15397	ED σ, MD π	$\Gamma_1 \rightarrow \Gamma_{3,4}$	$\Gamma_1 \rightarrow \Gamma_5$
	15411	ED π	$\Gamma_1 \rightarrow \Gamma_2$	$\Gamma_1 \rightarrow \Gamma_4$
$^5D_1 \rightarrow {}^7F_5$	15437			
	15454			
	15478			
	15493			
	15511			
$^5D_0 \rightarrow {}^7F_2$	15938	vibronic		
$^5D_1 \rightarrow {}^7F_4$	16008	ED π, MD σ	$\Gamma_{3,4} \rightarrow \Gamma_{3,4}$	$\Gamma_5 \rightarrow \Gamma_5$
	16033	ED σ, MD π	$\Gamma_1 \rightarrow \Gamma_{3,4}$	$\Gamma_2 \rightarrow \Gamma_5$
	16042	ED σ, MD π	$\Gamma_{3,4} \rightarrow \Gamma_2$	$\Gamma_5 \rightarrow \Gamma_4$
	16116	ED σ, MD π	$\Gamma_{3,4} \rightarrow \Gamma_2$	$\Gamma_5 \rightarrow \Gamma_3$
$^5D_0 \rightarrow {}^7F_2$	16120	ED π	$\Gamma_1 \rightarrow \Gamma_2$	$(\Gamma_1 \rightarrow \Gamma_3)$
$^5D_1 \rightarrow {}^7F_4$	16138	ED π	$\Gamma_1 \rightarrow \Gamma_2$	$\Gamma_2 \rightarrow \Gamma_3$
	16149	ED σ, MD π	$\Gamma_{3,4} \rightarrow \Gamma_1$	$\Gamma_5 \rightarrow \Gamma_2$
	16206	ED π, MD σ	$\Gamma_{3,4} \rightarrow \Gamma_{3,4}$	$\Gamma_5 \rightarrow \Gamma_5$
	16230	ED σ, MD π	$\Gamma_1 \rightarrow \Gamma_{3,4}$	$\Gamma_2 \rightarrow \Gamma_5$
$^5D_0 \rightarrow {}^7F_2$	16293	ED σ	$\Gamma_1 \rightarrow \Gamma_{3,4}$	$\Gamma_1 \rightarrow \Gamma_5$

(continued overleaf)

TABLE II. *(continued)*

Transition	$\bar{\nu}$ (cm^{-1})	Polarisation and mechanism	Identification	
			S_4	D_{2d}
	16379	ED π	$\Gamma_1 \rightarrow \Gamma_2$	$\Gamma_1 \rightarrow \Gamma_4$
$^5D_1 \rightarrow {}^7F_4$	16413	ED σ, MD π	$\Gamma_{3,4} \rightarrow \Gamma_1$	$\Gamma_5 \rightarrow \Gamma_1$
$^5D_0 \rightarrow {}^7F_1$	16840	MD σ	$\Gamma_1 \rightarrow \Gamma_1$	$\Gamma_1 \rightarrow \Gamma_2$
	16935	MD π	$\Gamma_1 \rightarrow \Gamma_{3,4}$	$\Gamma_1 \rightarrow \Gamma_5$
$^5D_1 \rightarrow {}^7F_3$	16982	ED σ, MD π	$\Gamma_{3,4} \rightarrow \Gamma_2$	$\Gamma_5 \rightarrow \Gamma_3$
	17002	ED π	$\Gamma_1 \rightarrow \Gamma_2$	$\Gamma_2 \rightarrow \Gamma_3$
	17067	ED π, MD σ	$\Gamma_{3,4} \rightarrow \Gamma_{3,4}$	$\Gamma_5 \rightarrow \Gamma_5$
	17089	ED σ, MD π	$\Gamma_1 \rightarrow \Gamma_{3,4}$	$\Gamma_2 \rightarrow \Gamma_5$
	17117	ED σ, MD π	$\Gamma_{3,4} \rightarrow \Gamma_1$	$\Gamma_5 \rightarrow \Gamma_2$
	17146	ED π, MD σ	$\Gamma_{3,4} \rightarrow \Gamma_{3,4}$	$\Gamma_5 \rightarrow \Gamma_5$
	17159	ED σ, MD π	$\Gamma_{3,4} \rightarrow \Gamma_2$	$\Gamma_5 \rightarrow \Gamma_4$
	17169	ED σ, MD π	$\Gamma_1 \rightarrow \Gamma_{3,4}$	$\Gamma_2 \rightarrow \Gamma_5$
	17183	ED π	$\Gamma_1 \rightarrow \Gamma_2$	$(\Gamma_2 \rightarrow \Gamma_4)$
$^5D_1 \rightarrow {}^7F_2$	17844	MD π	$\Gamma_{3,4} \rightarrow \Gamma_1$	$\Gamma_5 \rightarrow \Gamma_1$
	17868	MD σ	$\Gamma_1 \rightarrow \Gamma_1$	$\Gamma_2 \rightarrow \Gamma_1$
	17891	ED π	$\Gamma_1 \rightarrow \Gamma_2$	$\Gamma_2 \rightarrow \Gamma_3$
	18042	MD σ	$\Gamma_{3,4} \rightarrow \Gamma_{3,4}$	$\Gamma_5 \rightarrow \Gamma_5$
	18064	MD π	$\Gamma_1 \rightarrow \Gamma_{3,4}$	$\Gamma_2 \rightarrow \Gamma_5$
	18129	MD π	$\Gamma_{3,4} \rightarrow \Gamma_2$	$\Gamma_5 \rightarrow \Gamma_4$
$^5D_1 \rightarrow {}^7F_1$	18589	ED σ, MD π	$\Gamma_{3,4} \rightarrow \Gamma_1$	$\Gamma_5 \rightarrow \Gamma_2$
	18601	MD σ	$\Gamma_1 \rightarrow \Gamma_1$	$(\Gamma_2 \rightarrow \Gamma_2)$
	18685	ED π, MD σ	$\Gamma_{3,4} \rightarrow \Gamma_{3,4}$	$\Gamma_5 \rightarrow \Gamma_5$
	18709	MD π, ED σ	$\Gamma_1 \rightarrow \Gamma_{3,4}$	$\Gamma_2 \rightarrow \Gamma_5$
$^5D_1 \rightarrow {}^7F_0$	19019	MD π	$\Gamma_{3,4} \rightarrow \Gamma_1$	$\Gamma_5 \rightarrow \Gamma_1$
	19040	MD σ	$\Gamma_1 \rightarrow \Gamma_1$	$\Gamma_2 \rightarrow \Gamma_1$

a corresponding Γ_1 to Γ_2 (in S_4) transition, situated 21 cm^{-1} higher in energy, but this is not observed. As explanation one can suggest that this transition corresponds to the forbidden $\Gamma_2 \rightarrow \Gamma_4$ in D_{2d}.

The third $\Gamma_{3,4}$ to Γ_1 line should appear at about 15935 cm^{-1}, but is superposed on the vibronic transition at that wavenumber.

Region 14900–15300 cm^{-1} (Fig. 1c) → $^7F_5$

This region corresponds to the $^5D_1 \rightarrow {}^7F_5$ transition. The identification and position of Stark levels is hard to get: no comparison is possible since the $^5D_0 \rightarrow {}^7F_5$ transition is not observed. Moreover, the signal to noise ratio is very poor.

An attempt to assign the peaks is given in Table II, mainly based on the previous analysis and on the results of the crystal field calculation that simulates the presence of the Stark levels in this region.

The result of the identification of the electronic transitions is given in Table II. The experimental energy levels are given in Table III and Fig. 3.

Crystal Field Parametrisation

Due to the high degeneracy (3003) of the 4f^6 configuration, it is not practicable to diagonalize the full secular determinant, even if it can be reduced to three submatrices for the S_4 and D_{2d} symmetries. As the ground septet is well isolated and there are no other multiplets with that same multiplicity, the $|\,^7F_J>$ wavefunctions have a quite pure ^7F character (90 to 95%) and the J-mixing operates only within the multiplet. The calculation of the crystal field

TABLE III. Experimental and Calculated Energy Levels of Eu^{3+} in $LiYF_4$.

Multiplet	$\bar{\nu}_{exp}$ (cm^{-1})	$\bar{\nu}_{calc}$ (cm^{-1})	Symmetry assignment	
			D_{2d}	S_4
$^7F_0$	0	0	Γ_1	Γ_1
$^7F_1$	334	335	Γ_5	$\Gamma_{3,4}$
	430	429	Γ_2	Γ_1
$^7F_2$	891	888	Γ_4	Γ_2
	976	975	Γ_5	$\Gamma_{3,4}$
	1150	1150	Γ_3	Γ_2
	1172	1177	Γ_1	Γ_1
$^7F_3$	1859	1862	Γ_4	Γ_2
	1873	1872	Γ_5	$\Gamma_{3,4}$
	1903	1899	Γ_2	Γ_1
	1951	1952	Γ_5	$\Gamma_{3,4}$
	2038	2038	Γ_3	Γ_2
$^7F_4$	2606	2608	Γ_1	Γ_1
	2812	2813	Γ_5	$\Gamma_{3,4}$
	2870	2873	Γ_2	Γ_1
	2905	2903	Γ_3	Γ_2
	2978	2977	Γ_4	Γ_2
	3013	3010	Γ_5	$\Gamma_{3,4}$
	–	3074	Γ_1	Γ_1
$^7F_5$	3795	3787	Γ_3	Γ_2
	3807	3799	Γ_5	$\Gamma_{3,4}$
		3847	Γ_2	Γ_1
	3998	3995	Γ_5	$\Gamma_{3,4}$
		4011	Γ_1	Γ_1
		4014	Γ_2	Γ_1
	4050	4059	Γ_5	$\Gamma_{3,4}$
	4070	4074	Γ_4	Γ_2
$^5D_0$	(17270)	17257[a]	Γ_1	Γ_1
$^5D_1$	19019	19012[a]	Γ_5	$\Gamma_{3,4}$
	19040	19046[a]	Γ_2	Γ_1

[a]Calculated from the extended basis.

parameters can be performed accurately on this strongly reduced basis (49 × 49) when the calculated barycenters are adjusted to the experimental ones.

The crystal field potentials for D_{2d} and S_4 symmetries are:

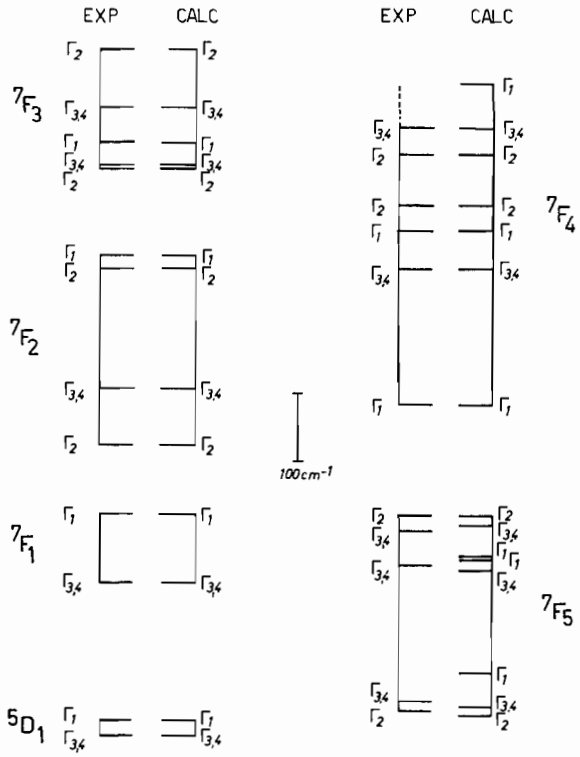

Fig. 3. Energy diagram of $LiYF_4/Eu^{3+}$ in a S_4 symmetry.

$$D_{2d}: H^{even} = B_0^2C_0^2 + B_0^4C_0^4 + B_4^4(C_4^4 + C_{-4}^4) + B_0^6C_0^6 + B_4^6(C_4^6 + C_{-4}^6)$$

$$H^{odd} = i\,B_2^3(C_2^3 - C_{-2}^3) + i\,B_2^5(C_2^5 - C_{-2}^5) + i\,B_2^7(C_2^7 - C_{-2}^7) + i\,B_6^7(C_6^7 - C_{-6}^7)$$

$$S_4: H^{even} = H_{D_{2d}}^{even} + i\,B_4^4(C_4^4 - C_{-4}^4) + i\,B_4^6(C_4^6 - C_{-4}^6)$$

$$H^{odd} = H_{D_{2d}}^{odd} + B_2^3(C_2^3 + C_{-2}^3) + B_2^5(C_2^5 + C_{-2}^5) + B_2^7(C_2^7 + C_{-2}^7) + B_6^7(C_6^7 + C_{-6}^7)$$

The number of even c.f.p. for S_4 can be reduced to six if $i\,B_4^4$ is set to zero by an appropriate choice of the reference axis system.

Different c.f.p. determinations have been performed for this crystalline matrix, with different rare earth doping ions, and including or not the imaginary $i\,B_4^6$ parameter. Results are summarized in ref. 2. For the Eu^{3+} case we considered values extrapolated from the literature as starting parameters. These parameters were slightly modified in order to simulate more correctly the observed splittings: B_0^2 for the $^7F_1$ splitting, B_0^4 and B_4^4 for $^7F_2$ and other parameters for $^7F_3$ and $^7F_4$.

Therefore, the final refining procedure runs rapidly towards a low r.m.s. (3 cm^{-1}) with a correct

assignment to the irreducible representations. The c.f.p. values are:

B_0^2: 349 (±3) cm^{-1}

B_0^4: −728 (±4) cm^{-1}

B_4^4: −919 (±3) cm^{-1}

B_0^6: −35 (±6) cm^{-1}

B_4^6: −790 (±4) cm^{-1}

iB_4^6: 216 (±9) cm^{-1}

The signs of B_4^4 and B_4^6 are reversed from all other calculations. This feature does not modify at all the energy level positions, but permutes the B_1 and B_2 irreducible representations. This has to be related to the relative weakness of certain transitions, which are allowed when the symmetry is S_4 but forbidden if the approximative D_{2d} symmetry is considered.

Moreover, it has been shown elsewhere that some configuration truncation [9, 10] could be considered if one wants to simulate correctly the excited $^5D_0$, $^5D_1$ and $^5D_2$ level positions together with ^7F_J, and to derive the complete wave functions associated with these levels. By using the calculated c.f.p. values given above (with i B_4^6 set to zero), this procedure allows an estimation of the free ion parameters. The derived values are: E_0 = 2880 cm^{-1}, E_1 = 5544 cm^{-1}, E_2 = 24.83 cm^{-1}, E_3 = 585 cm^{-1}, α = 20 cm^{-1}, β = −640 cm^{-1}, γ = 1750 cm^{-1} and ζ = 1285 cm^{-1}.

Conclusion

This paper reports a spectroscopic study on the $LiYF_4$ crystal, doped with the Eu^{3+} ion. Whereas several studies have been published on the $LiYF_4$ doped with other ions [2, 12–15], this is to our knowledge the first time that Eu^{3+}-doped crystals were grown with size and quality adequate for optical measurements.

In this paper the fluorescence spectrum has been analyzed and accurately described by a set of parameters whose order of magnitude and sign fit rather well in the list of those recently reported in the review by Morrison and Leavitt [2].

Nevertheless, the particular case of Eu^{3+} gives more precision about the sign of some crystal field parameters.

The reverse of the sign of the B_4^4 and B_4^6 parameters with respect to those given by other authors [1, 2], does not modify the energy level scheme but permutes the B_1 and B_2 crystal field representations. The wave functions associated with these levels also show inversions in the sign of some of their components. The magneto-optical measurements should help us in solving this problem.

Our interest for the $LiYF_4/Eu^{3+}$ crystal is mainly motivated by its parentage with the KY_3F_{10}/Eu^{3+} crystal. This is one of the few examples where the phase diagram allows that a same ion (Eu^{3+}) complexed with a same ligand (F^-) can be studied in two different site symmetries namely D_{2d} for $LiYF_4$ and C_{4v} for KY_3F_{10}. A complete study of the KY_3F_{10}/Eu^{3+} has been published [16–18].

A prospective comparison between the magneto-optical spectra of both compounds allows us to state that the sign inversion predicted theoretically in previous papers between the C_{4v} and D_{2d} symmetry [3, 19] is indeed found experimentally.

Acknowledgements

This work was supported through grants from the IWONL and FKFO Belgium. The authors are indebted to the Belgian Government (Programmatie van het Wetenschapsbeleid).

References

1 N. Karayianis and C. A. Morrison, 'Rare Earth Ion-Host Crystal Interaction. 1. Point Charge Lattice Sum in Scheelites', HDL-TR-1648, 1973.
2 C. A. Morrison and R. P. Leavitt, 'Handbook on the Physics and Chemistry of Rare Earths, Vol. 5', 1982, p. 461.
3 C. Görller-Walrand and J. Godemont, *J. Chem. Phys., 66,* 48 (1977).
4 C. Görller-Walrand and W. Colen, *Inorg. Chim. Acta, 84,* 183 (1984).
5 I. Laursen and L. M. Holmes, *J. Phys. C:, 7,* 3765 (1974).
6 W. Urland, *Chem. Phys. Lett., 77,* 1, 58 (1983).
7 G. F. Koster, J. O. Dimmock, R. G. Wheeler and H. Statz, 'Properties of the 32 pointgroups', M.I.T., 1963.
8 F. A. Cotton, 'Chemical applications of group theory', Wiley, 1963.
9 J. Hölsa and P. Porcher, *J. Chem. Phys., 75,* 5, 2108 (1981).
10 J. Huang, J. Loriers, P. Porcher, G. Teste de Sagey, C. Lévy-Clément and P. Caro, *J. Chem. Phys., 80,* 12, 6204 (1984).
11 R. E. Thoma, G. D. Brunton, R. A. Penneman and T. K. Koenan, *Inorg. Chem., 9,* 1096 (1970).
12 L. Esterowitz, F. J. Bartoli and R. E. Allen, *J. Lumin., 21,* 1 (1979).
13 H. P. Christensen, *Phys. Rev. B:, 17,* 10, 4060 (1978).
14 H. P. Christensen, *Phys. Rev. B:, 19,* 12, 6564 (1979).
15 H. P. Christensen, *Phys. Rev. B:, 19,* 12, 6573 (1979).
16 P. Porcher and P. Caro, *J. Chem. Phys., 65,* 1, 89 (1976).
17 P. Porcher and P. Caro, *J. Chem. Phys., 68,* 9, 4176 (1978).
18 P. Porcher and P. Caro, *J. Lumin., 21,* 207 (1980).
19 C. Görller-Walrand and Y. Beyens, 'The Rare Earth in Modern Science and Technology, Vol. 2', 1980, p. 87.